PROCEEDINGS OF SPIE

Measurement of human eye aberrations using an optical simulator based on pyramid wavefront sensor

Wang, Chaoyan, Chen, Xinyang, Zheng, Zheng, Bu, Zhaohui, Cai, Jianqing, et al.

Measurement of human eye aberrations using an optical simulator based on pyramid wavefront sensor

Chaoyan Wang[1,a] *, Xinyang Chen[1,b], Zheng Zheng[2,c], Zhaohui Bu[2,d], Jianqing Cai[1,e],

Yuanyuan Ding[1,f], Bei Wang[3,g]

[1]Shanghai Astronomical Observatory, 80 Nandan Road, Shanghai, 200030, China

[2]University of Shanghai for Science and Technology, 516 Jungong Road, Shanghai, 200093, China

[3]Shanghai Laisi Information Technology Co., Ltd., 1158 Zhongxin Road, Shanghai, 201615, China

[a] *superyan@shao.ac.cn, [b]xychen@shao.ac.cn, [c]zhengzhengnew@icloud.com,

[d]buzh@shao.usst.edu.cn, [e]jqcai@shao.ac.cn, [f]yuanyuand@shao.ac.cn,

[g]cekongwangbei@163.com

ABSTRACT

In general, most of the adaptive optical systems for human eye aberration detection are based on the wavefront slope measurement provided by the Shark-Hartman wavefront sensor (SHWS), and then the wavefront slope is fed back to the deformable mirror to correct the human eye aberrations. Compared with the SHWS, the pyramid wavefront sensor (PWS) has the characteristics of fast sampling speed, wide linear capture range, and high sensitivity. Our works show that the modulation angle of the dynamic high-frequency modulator affects the dynamic measurement range, linearity and sensitivity of the pyramid sensing. The dynamic measurement range and the linear fitting residuals are both proportional to the modulation angle, and the sensitivity is inversely proportional to the modulation angle. Pixel combination affects the sensitivity of the detection signals of the pyramid sensor. The pixel combination mode of 1×1, 2×2, and 3×3 is tested respectively. When the pixel combination mode of 2×2 is used, the sensitivity of the signals will be highest significantly. In addition, the beacon light used to detect the human eye should not be too strong. The grinding "blind zone" of the spires and edges will have a scattering effect on the incident light and cause loss of light energy. Therefore, it is necessary to optimize the parameters of the pyramid sensor and further improve the processing technology of the pyramid prism.

Keywords：Pyramid wavefront sensor, Human eye aberrations, Wavefront slope

1 INTRODUCTION

High resolution imaging of retinal cell can do benefit to the early diagnosis of retinopathy inducing retinal vascular disease, macular disease and detached retinas. However, human eyes ought to be regarded as a complex non-ideal optical system. Whether normal eyes or ill eyes, both contain low-order and high-order aberrations and cause vision degradation[1]. The development of wavefront sensing technology provides the possibility of correcting human eye aberrations. The Shack-Hartman wavefront sensor (SHWS) is the most popular sensor for detecting human eye aberrations, and is widely used in the AO system[2]. However, the Shack-Hartman wavefront detector obtains the local slope of the wavefront at each micro lens aperture, without considering the imaging quality of the micro lens array. If the spot pattern formed by the micro lens becomes blurred or due to the wavefront distortion leads to the overlapped bitmap, so the wavefront reconstruction will become difficult[3]. During recent years, some new wavefront techniques for detecting human eye aberrations have emerged.

Among them, the pyramid wavefront sensor (PWS) used by astronomers to measure wavefront aberrations due to atmospheric turbulence is becoming a hot spot[3][4]. Because of its advantages of sampling in pupil and adjustable dynamic range, it was introduced into ophthalmic optics and showed its huge practical value[5].

In Section 2, a basic principle of PWS is described firstly. A detailed scheme of an optical simulator for human eye aberrations is expounded in Section 3. Utilizing this simulator, defocus and astigmatism, the two main components of human eye aberrations have been detected by PWS successful. Relevant measurements are described in Section 4. Finally, a conclusion and future consideration are given in Section 5.

2 BASIC PRINCIPLE OF PWS

Figure 1 shows a schematic diagram of a pyramid wavefront sensor. After the incident collimated light is converged onto the apex of the pyramid prism by a lens. Then the focused beam passed through the pyramid prism is divided into four sub beams. A camera with a relay lens is used to obtain four sub-pupil images respectively. Each point of pupil is conjugated with the corresponding sample pixel of each sub-pupil image on same position. If the system has no aberrations, the four spots are of the same intensity. Otherwise, their intensities will no longer be equal. From the intensity difference between these spots, the wavefront slope can be calculated[6].

As shown in Figure 1, there is a tip/tilt mirror between the lens and the pyramid prism. This mirror will produce a spacial angle modulation in the orthogonal direction respect to the prism edge. It can increase the dynamical range of the sensor remarkably[7].
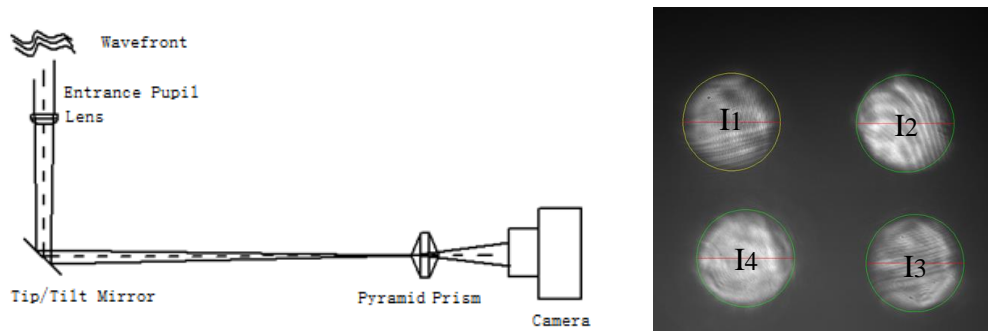

Fig.1 A schematic diagram of a pyramid wavefront sensor.

Given that the intensities of the four pixels in the sub-pupil images are marked as $I_{1\sim4}$, S_X and S_Y of the responding spot on the entrance pupil in the x and y directions are defined according to formulas (1) and (2). The relationship between wavefront slope with S_X and S_Y is implied by formula (3), where α is amplitude angle of modulation. Wavefront aberrations can be reconstructed based on the Zernike polynomial as shown with formulas (4), which is also as same as the method for SHWS wavefront reconstruction[8].

$$S_x(i,j) = \frac{I_1(i,j)+I_4(i,j)-I_2(i,j)-I_3(i,j)}{I_1(i,j)+I_2(i,j)+I_3(i,j)+I_4(i,j)} \qquad (1)$$

$$S_y(i,j) = \frac{I_1(i,j)+I_2(i,j)-I_3(i,j)-I_4(i,j)}{I_1(i,j)+I_2(i,j)+I_3(i,j)+I_4(i,j)} \qquad (2)$$

$$\begin{cases} \frac{\partial W(i,j)}{\partial x} \propto \alpha \cdot \sin[\frac{\pi}{2}S_x(i,j)] \\ \frac{\partial W(i,j)}{\partial y} \propto \alpha \cdot \sin[\frac{\pi}{2}S_y(i,j)] \end{cases} \qquad (3)$$

$$W(r) = \Sigma_j^n a_j Z_j(r) \qquad (4)$$

3 DESIGN OF AN OPTICAL SIMULATOR

In order to simulate the optical aberrations which is similar to human eyes and verify the feasibility and effectiveness of PWS applied to aberrations measurement[9], we design an optical simulator shown as Figure 2. The light generated by a slit lamp passes through a serial of converagence, shrinking and folding from L1-L3 lenslets and M1 mirrors, and is

propagated to M2 and M3 mirrors which are mounted on a movable translation stage. This stage drived by piezoelectric ceramic will move along light propagation direction, which is simulated to produce a defous item of human eye aberrations. Next, The reflected beam is collimated by lens L4 and arrives at a 109-channels deformable mirror (DM) which will produce another astigmatism item of human eye aberrations. In order to match the entrance pupil of SHWS and PWS, the following beam's diameter is reduced again by L5 and L6 lens. SHWS plays a role on both calibrating static optical errors of the whole simulator and validating the measurement of PWS. L7, M5, Pyramid and camera have been introduced in Section 2.
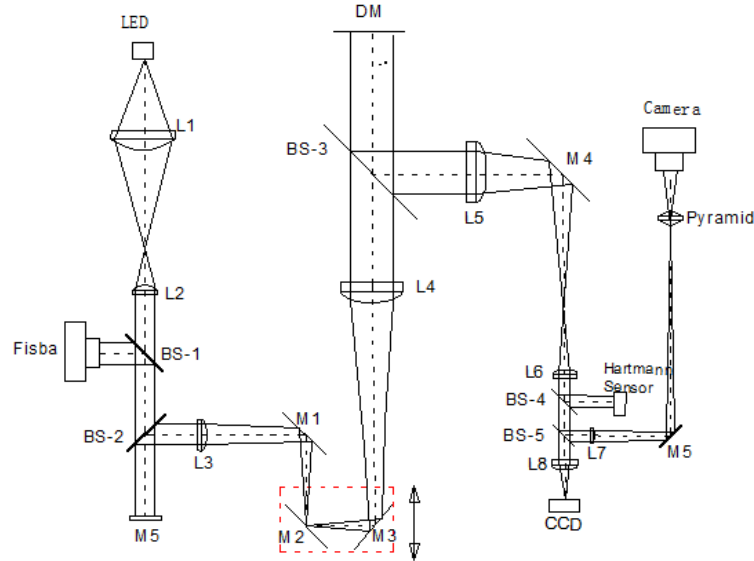

Fig.2 The optical layout of simulator

4 MEASUREMENT RESULTS

4.1 Defocus

Defocus is the fourth item of human eye aberrations expressed with Standard Zernike Polynomial. This error component occupys the largest percentage of human eye aberrations and can reach at least 20μm if eye'pupil is 6mm[1]. We choose a translating stage with enough large travel range. The stage moved step by step with a small step length. Meanwhile at each step, PWS captured the correponding sub-pupil image and reconstruct the defocus coefficient. We also did some comparative measurements in case of change modulation amplitude or binning mode of camera.
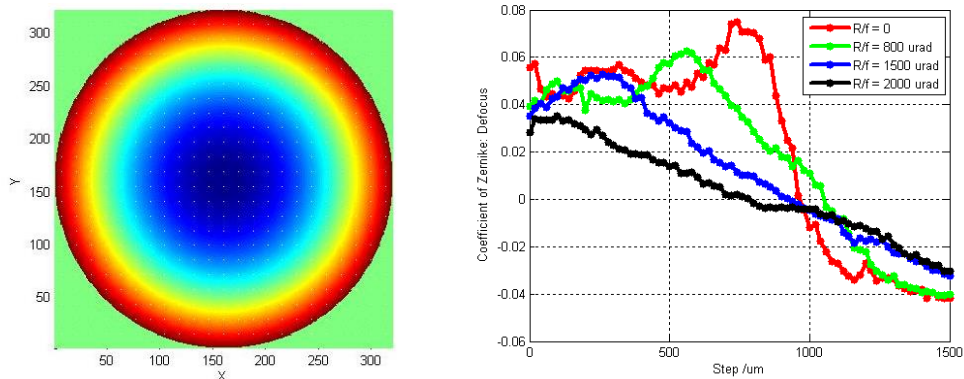

Fig.3 Left: Phase diagram of defocus expressed with Standard Zernike Polynomial; Right: Reconstructed defocus coefficient relative to travel of translating stage

Figure 3 shows profiles of reconstructed defocus coefficient with respect to travel of translating stage under different modulation amplitude. It implies there is a nearly linear relationship between reconstructed defocus coefficient and monotonically increasing defocus by moving the stage along the light axis. It means PWS can be available to measure defocus error after being well calibrated. Following with increasing the modulation amplitude (R/f), the valid linear region of measurement is becoming more wider. On the contrary, the sensitivity of measurement would be reduced. A quantitative comparation is seen in Table 1.

Table 1 Specifications of defocus measured by PWS

Modulation Ampitude (µrad)	Linear Range (µm)	Fitting Residual RMS within Linear Range	Sensitivity (µm^{-1})
0	~420	0.0082	3.094×10^{-4}
800	~840	0.0031	1.283×10^{-4}
1500	~1240	0.0031	6.875×10^{-5}

Another test was carried out to confirm whether different binning mode of the camera would affect the sensitivity of mensurement. Figure 4 is the test result based on three binning modes: 1×1, 2×2 and 3×3. It has implied that binning 2×2 is the most optimal mode because of its highest sensitivity.
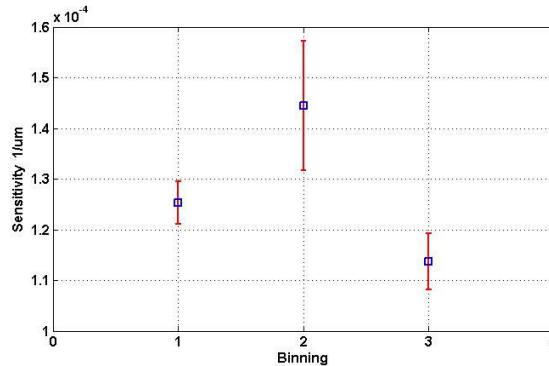

Fig.4 Sensitivity of measurement based on different binning modes of camera

4.2 Astigmatism

Astigmatism also is main component of human eye aberrations. A 109-channels deformable mirror is utilized to produce astigmatism error. Firstly, This deformable mirror has corrected the static optical errors of this simulator's light path to below 0.06λ ($\lambda = 0.633\mu m$). Astigmatism is expressed as the second order Zernike item $a_4 Z_2^{-2}(\rho, \theta)$ ($45°$ astigmatism) and $a_6 Z_2^2(\rho, \theta)$ ($0°$ astigmatism). Here we only illustrate the $0°$ astigmatism since these two item are similar. When the surface commands are outputed to deformable mirror, Zernike coefficient a_6 is increased step by step and the step length equals to $0.1\mu m$.
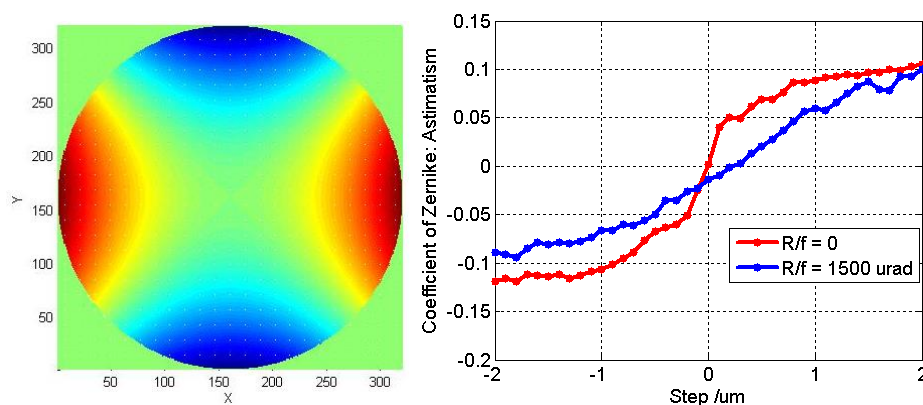

Fig.5 Left: Phase diagram of $0°$ astigmatism expressed with Standard Zernike Polynomial; Right: Reconstructed astigmatism coefficient relative to astigmatism coefficient which is imposed on deformable mirror

Figure 5 shows profiles of reconstructed astigmatism coefficient with respect to astigmatism coefficient which is imposed on deformable mirror with modulation amplitude = 0 and 1500μrad respectively. Similar to the measurement of defous, also there is a nearly linear relationship between command value and reconstructed value. Modulation can increase linear range of measurement, and the sensitivity of measurement is reduced on the contrary.

Table 2 Specifications of astigmatism measured by PWS

Modulation Ampitude (μrad)	Linear Range (μm)	Fitting Residual RMS within Linear Range	Sensitivity (μm^{-1})
0	±0.5	0.013	0.161
1500	±2	0.010	0.054

5 CONCLUSION

Our study has proved that human eye aberrations with large stroke such as defocus and astigmatism items can be detected by pyramid wavefront sensor effectively.Through more measurements based on the optical simulator, we find out further the dynamic measurement range and the linear fitting residuals are both proportional to the modulation amplitude, and the sensitivity is inversely proportional to the modulation amplitude. Binning parameter of camera would affect the sensitivity of the sensing signals of the pyramid sensor. So an optimized strategy is to extend the linear measurement range as far as possible through spacial modulation, and then choose optimal binning mode to improve measurement sensitivity.

The next work is to build an adaptive optics closeloop system to compensate human eye aberrations rapidly. A modal eye as a measurement target will be inserted the optical path of simulator. optimization of the pyramid sensor and further improvement of the processing technology for the pyramid prism are also necessary.

References

[1] Zhang Y. D., Rao C. H., Li X. Y., [Adaptive Optics and Laser Control], National Defence Industry Press, Beijing, 325-341 (2016)

[2] Roddier F., [Adaptive Optics in Astronomy], Cambridge University Press, Cambridge, 98-101 (1999)

[3] Riccardi A., Bindi N., Ragazzoni R., Esposito S., Stefanini P., "Laboratory characterization "Foucault-like wavefront sensor for Adaptive Optics", Proc. SPIE 3353, (1998)

[4] Zhu N. H., Chen X. Y., Zhou D., Cao J., J., "Study on measuring piston error of segmented mirror using pyramid sensor", Chinese Journal of Sensor and Actuators, 22(3), 433-437 (2009)

[5] Iglesias R., Ragazzoni R., Julien Y., Artal P., "Extended source pyramid wave-front sensor forthe human eye", Optics Express, 10(9), 419-428 (2002)

[6] Ragazzoni R., "Pupil plane wavefront sensing with oscillating prism", J. Modern Opt., 43, 289-293 (1996)

[7] Chen X. Y., Zhu N. H., "The design of software simulation based on pyramid wavefront sensor", Progress on Astronomy, 24(4), 362-272 (2006)

[8] Chamot S. R., Dainty C., Esposito S., "Adaptive optics for ophthalmic applications using a pyramid wavefront sensor", Optics Express, 14(2), 518-526 (2006)

[9] Akondi V, Jewel A. R., Vohnsen B, "Closed-loop adaptive optics using a spatial light modulator for sensing and compensating of optical aberrations in ophthalmic applications", Journal of Biomedical Optics, 19(9), 096014-1:7 (2014)